Monthly Notices
of the
ROYAL ASTRONOMICAL SOCIETY

MNRAS **472,** 1300–1314 (2017)
Advance Access publication 2017 July 26

doi:10.1093/mnras/stx1793

Multiwavelength observations of the 2015 nova in the Local Group irregular dwarf galaxy IC 1613

S. C. Williams,[1,2]★ M. J. Darnley[2] and M. Henze[3]

[1]*Physics Department, Lancaster University, Lancaster, LA1 4YB, UK*
[2]*Astrophysics Research Institute, Liverpool John Moores University, IC2 Liverpool Science Park, Liverpool, L3 5RF, UK*
[3]*Institute of Space Sciences (IEEC-CSIC), Campus UAB, Carrer de Can Magrans, s/n 08193 Barcelona, Spain*

Accepted 2017 July 13. Received 2017 July 12; in original form 2017 May 22

ABSTRACT

A nova in the Local Group irregular dwarf galaxy IC 1613 was discovered on 2015 September 10 and is the first nova in that galaxy to be spectroscopically confirmed. We conducted a detailed multiwavelength observing campaign of the eruption with the Liverpool Telescope, the LCO 2 m telescope at Siding Spring Observatory, and *Swift*, the results of which we present here. The nova peaked at $MV = -7.93 \pm 0.08$ and was fast-fading, with decline times of $t_{2(V)} = 13 \pm 2$ and $t_{3(V)} = 26 \pm 2$ d. The overall light-curve decline was relatively smooth, as often seen in fast-fading novae. *Swift* observations spanned 40–332 d post-discovery, but no X-ray source was detected. Optical spectra show the nova to be a member of the hybrid spectroscopic class, simultaneously showing Fe II and N II lines of similar strength during the early decline phase. The spectra cover the eruption from the early optically thick phase, through the early decline and into the nebular phase. The Hγ absorption minimum from the optically thick spectrum indicates an expansion velocity of 1200 ± 200 km s^{-1}. The full width at half-maximum of the Hα emission line between 10.54 and 57.51 d post-discovery shows no significant evolution and remains at $\sim$1750 km s^{-1}, although the morphology of this line does show some evolution. The nova appears close to a faint stellar source in archival imaging; however, we find the most likely explanation for this is simply a chance alignment.

Key words: novae, cataclysmic variables – ultraviolet: stars.

1 INTRODUCTION

Classical novae (CNe) are binary systems (Walker 1954; Kraft 1964) with a white dwarf (WD) accreting matter from a non-degenerate companion star (either main-sequence, sub-giant or red giant; see e.g. Darnley et al. 2012). As material builds up on the surface of the WD, the pressure and temperature increase until nuclear fusion occurs, leading to a thermonuclear runaway (Starrfield et al. 1972). This causes a rapid increase in luminosity, with the most luminous CN eruptions exceeding $M_V = -10$ (Shafter et al. 2009, Williams et al. in preparation). By definition, novae with one observed eruption are classified as CNe; those with two or more observed eruptions are classified as recurrent novae (RNe). The shortest recurrence period observed to date is 1 yr, in M31N 2008-12a (see e.g. Darnley et al. 2016). For detailed reviews of the nova phenomenon, see Bode & Evans (2008) and Woudt & Ribeiro (2014).

Novae have long been considered as potential Type Ia supernova (SN Ia) progenitor candidates (e.g. Whelan & Iben 1973), with the latest models indicating that WDs in nova systems can indeed gain mass over a long series of eruption cycles and eventually produce a SN Ia (Hillman et al. 2016). While it is widely accepted that SNe Ia are caused by thermonuclear explosions of carbon-oxygen WDs (Hoyle & Fowler 1960; Nomoto, Thielemann & Yokoi 1984; Hillebrandt & Niemeyer 2000; Nugent et al. 2011), the mechanism via which the WD reaches the critical mass to explode is still unclear (see Maoz, Mannucci & Nelemans 2014 for a detailed review of SN Ia progenitor candidates). Although the production of lithium in nova eruptions has been predicted for some time (e.g. Arnould & Norgaard 1975; Starrfield et al. 1978; Hernanz et al. 1996), observational evidence has recently been found that novae may contribute the majority of the ^{7}Li in the Galaxy (Izzo et al. 2015; Tajitsu et al. 2015, 2016; Molaro et al. 2016).

While it is generally not possible to study individual extragalactic novae in as much detail as their Galactic counterparts, there are several advantages to observing extragalactic novae. The large uncertainties in distance that can be associated with Galactic novae are largely negated when studying extragalactic populations and a better representation is given of an entire galaxy's nova population. Additionally, it enables the studies of novae in different environments, for example the stellar populations of the nearby dwarf galaxies, the Large Magellanic Cloud (LMC) and Small Magellanic Cloud

★ E-mail: s.williams7@lancaster.ac.uk

(SMC) are very different from the large spirals like M31 and our own Galaxy.

Many Local Group novae are discovered each year, yet to date detailed studies of individual nova eruptions in the low-metallicity environments typically found in dwarf irregular galaxies have been restricted to the nearby Magellanic Clouds (MCs). Dwarf galaxies of course have low nova rates, with the nova rates of the LMC and SMC calculated to be 2.4 ± 0.8^{-1} and $0.9 \pm 0.4\,\mathrm{yr}^{-1}$, respectively (Mróz et al. 2016). This compares to rates of $65^{+16}_{-15}\,\mathrm{yr}^{-1}$ in M31 (Darnley et al. 2006), $33^{+13}_{-8}\,\mathrm{yr}^{-1}$ in M81 (Neill & Shara 2004), and even as high as $363^{+33}_{-45}\,\mathrm{yr}^{-1}$ in M87 (Shara et al. 2016). To build a full picture of how the properties of novae depend on the properties of their host galaxy, it is important that we study nova eruptions in these dwarf irregulars in as much detail as possible.

IC 1613 is an irregular dwarf galaxy in the Local Group at a distance of approximately 730 kpc (Scowcroft et al. 2013; Menzies, Whitelock & Feast 2015). Recent evidence suggests that it has a metallicity of about one fifth of Solar, similar to that of the SMC (Garcia et al. 2014; Bouret et al. 2015), and its star formation rate has been constant over time (Skillman et al. 2014). IC 1613 differs from the MCs as it is essentially isolated, whereas the MCs are interacting with the Milky Way (see van den Bergh 2000 for an overview).

A total of three nova candidates have previously been discovered in IC 1613. The first was imaged at $B \simeq 17.5$ on three plates taken on a single night by Walter Baade in 1954 November, having not been visible the night before and no further images were taken that season (Sandage 1971). The second candidate was detected on 1996 October 12, although the eruption time of this candidate is poorly constrained, with the last non-detection being 2 months prior (Mantegazza et al. 2001). For 9 d following October 12, the candidate was seen to decline in brightness (Mantegazza et al. 2001). The third and most recent nova candidate was discovered in 1999 (King, Modjaz & Li 1999), but this was actually a Mira variable (Kurtev et al. 2001).

Nova IC 1613 2015 (PNV J01044358+0203419) was discovered at $01^{\mathrm{h}}04^{\mathrm{m}}43^{\mathrm{s}}.58\ +02^{\circ}03'41''.9$ with an unfiltered magnitude of 17.5 on 2015 September 10.48 UT, with nothing visible down to a limiting magnitude of about 18.0 on September 9 (Halevi, Zheng & Filippenko 2015), by the Lick Observatory Supernova Search (see Filippenko et al. 2001 for further details). After classification as an extragalactic nova (Williams & Darnley 2015), we conducted optical, near-IR, near-UV and X-ray observations of the eruption, which we present in this paper.

2 OBSERVATIONS AND DATA ANALYSIS

2.1 Ground-based photometry

Nova IC 1613 2015 was initially followed with IO:O,[1] the optical imager on the 2 m Liverpool Telescope on La Palma, Canary Islands, Spain (LT; Steele et al. 2004), using B, V and i' filters, with the first set of observations taken 1.61 d after discovery on 2016 September 12.09 UT. Once the nova nature of the object became clear, the filter set was expanded to u', B, V, r', i' and z'. We also began monitoring the eruption in the near-IR using the fixed H-band filter on the IO:I imager on the LT (Barnsley et al. 2016). In addition to the LT data, we also obtained some photometric observations through B, V, r' and i' filters using the Las Cumbres Observatory (LCO) 2 m telescope at Siding Spring Observatory, New South Wales, Australia (formally the Faulkes Telescope South, FTS; Brown et al. 2013). An IO:O image of the nova in eruption is shown in Fig. 1.

The $u'BVr'i'z'$ photometry was calculated using aperture photometry in GAIA[2] and calibrated against field stars from the Sloan Digital Sky Survey Data Release 9 (Ahn et al. 2012). The B and V magnitudes of these calibration stars were calculated using the transformations in Jordi, Grebel & Ammon (2006). The H-band observations were calibrated against different stars from the 2MASS All Sky Catalog of point sources (Cutri et al. 2003).

[1] http://telescope.livjm.ac.uk/TelInst/Inst/IOO

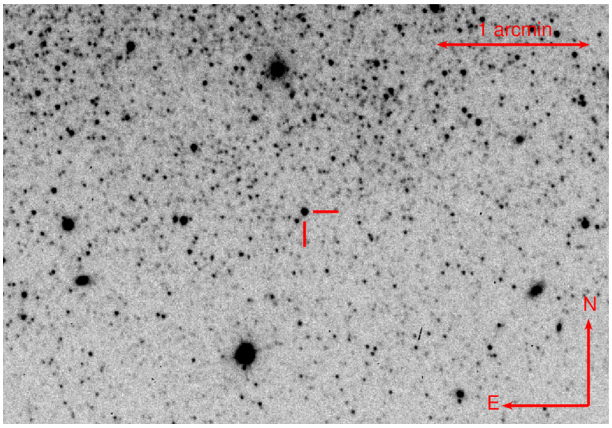

Figure 1. Negative image of Nova IC 1613 2015 in eruption taken through an r'-band filter with IO:O on the LT on 2015 October 9.00 UT. The position of the nova is indicated by the red lines near the centre of the image.

Table 1. Summary of all spectroscopic observations of Nova IC 1613 2015 with the SPRAT spectrograph on the LT.

Date (UT)[a]	Days post-discovery	Exposure time (s)
2015 September 12.07	1.59	1800
2015 September 17.07	6.59	1800
2015 September 21.02	10.54	1800
2015 September 25.09	14.61	1800
2015 October 07.03	26.55	3600
2015 November 06.99	57.51	5400

Note. [a] The date listed here refers to the mid-point of each observation.

2.2 Spectroscopy

The optical spectra were taken using the SPectrograph for the Rapid Acquisition of Transients (SPRAT), a low-resolution high-throughput spectrograph on the LT (Piascik et al. 2014). It has a 1″.8 slit width, giving a resolution of 18 Å. Our observations were all taken using the blue-optimized mode. The details of the spectra are summarized in Table 1.

Spectrophotometric standards were not observed at similar times as the IC 1613 spectroscopy, but we observed the standard G191-B2B using the same SPRAT instrument set-up on 2015 December 17, 2015 December 30 and 2016 January 10. The flux calibration

[2] GAIA is a derivative of the Skycat catalogue and image display tool, developed as part of the VLT project at ESO. Skycat and GAIA are free software under the terms of the GNU copyright.

Table 2. *Swift* UVOT magnitude and X-ray upper limits.

ObsID	Exp[a] (ks)	Date[b] (UT)	MJD[b] (d)	Δt[c] (d)	UV[d] (mag) *UVW1*	*UVM2*	*UVW2*	Rate (10^{-3} ct s^{-1})	$L_{0.2-1.0}^{e}$ (10^{37} erg s^{-1})
00034085001	4.6	2015-10-20.54	57315.55	40.07	18.6 ± 0.1	–	–	<4.2	<2.3
00034085002	4.2	2015-11-08.29	57334.29	58.81	19.6 ± 0.1	–	–	<2.6	<1.5
00034085003	4.6	2015-11-29.22	57355.23	79.75	20.2 ± 0.2	–	–	<5.5	<3.1
00034085004	4.1	2016-01-08.04	57395.05	119.57	20.9 ± 0.3	–	–	<2.1	<1.2
00034085005	4.0	2016-02-09.09	57427.09	151.61	>20.9		–	<3.2	<1.8
00084201006	1.3	2016-02-17.81	57435.81	160.33	>19.5	>19.8	>20.0	<8.7	<4.8
00084201007	6.5	2016-05-26.43	57534.44	258.96	>20.1	>20.8	>21.1	<1.8	<1.0
00084201008	0.9	2016-05-28.90	57536.90	261.42	>19.3	>19.6	>19.8	<9.5	<5.3
00034085006	2.4	2016-08-07.07	57607.07	331.59	>21.0	–	–	<4.9	<2.7

Notes. [a]Dead-time corrected XRT exposure time.
[b]Start date of the observation.
[c]Time in days after the eruption on 2015-09-10.48 UT (MJD 57275.48).
[d]Vega magnitudes for the *UVW*1, *UVM*2 and *UVW*2 filters with central wavelength: 2600, 2250 and 1930 Å, respectively.
[e]X-ray luminosity upper limits (unabsorbed, blackbody fit, 0.2–1.0 keV) were estimated according to Section 2.3.

of each spectrum was performed using standard routines in IRAF[3] (Tody 1986). The standard observations were calibrated against data from Oke (1990) obtained via ESO. Due to different observing conditions, and particularly seeing losses and atmospheric conditions (i.e. cloud), the absolute flux calibrations of each spectrum can vary significantly. Examining the standard star observations discussed above, we estimate this causes the typical flux calibration error (at 5000 Å) to be of order 15–20 per cent. However, the relative calibration across any individual spectrum (i.e. between red and blue, after removing the systematic flux calibration offset) should be relatively good with the uncertainties <10 per cent.

2.3 *Swift* observations

The supersoft X-ray source (SSS) phase in novae is caused by nuclear burning of hydrogen on the surface of the WD. The SSS emission can be detected once the ejecta become optically thin to X-rays and the SSS 'turn-off' is thought to represent the end of nuclear burning (see e.g. Krautter et al. 1996).

We were granted six *Swift* (Gehrels et al. 2004) target of opportunity (ToO) observations (target ID 34085) to follow the UV and X-ray evolution of the nova. Additionally, we analysed data aimed at IC 1613 itself (target ID 84201), which includes our object in the field of view. All *Swift* data are summarized in Table 2.

The *Swift* UV/optical telescope (UVOT, Roming et al. 2005) data were reduced using the HEASoft (v6.16) tool `uvotsource`. The UVOT magnitudes are based on aperture photometry of carefully selected source and background regions. The photometric calibration assumes the UVOT photometric (Vega) system (Poole et al. 2008) and have not been corrected for extinction. The central wavelengths of the utilized UVOT filters are: *UVW1*: 2600 Å; *UVM2*: 2250 Å; *UVW2*: 1930 Å.

All *Swift* X-ray telescope (XRT; Burrows et al. 2005) data were obtained in the photon counting (PC) mode. For extraction of the count rate upper limits we made use of the on-line interface[4] of Evans et al. (2009). This tool uses the Bayesian formalism of Kraft, Burrows & Nousek (1991) for low numbers of counts. As is recommended for SSSs, only grade zero events were extracted. To convert the counts to X-ray fluxes we assume a conservative (maximum) blackbody temperature of 50 eV and a Galactic foreground absorption of $N_{\rm H} = 3 \times 10^{20}$ cm^{-2}. The absorption was derived from the HEASARC $N_{\rm H}$ tool based on the hydrogen maps of Dickey & Lockman (1990).

We estimated the X-ray temperature based on the reference frame of the M31 SSS nova sample and the correlations subsequently found by Henze et al. (2014a). In M31, a t_2 of 13 d (see Section 3.1) would correspond to an SSS phase from about days 60 to 200, which in turn suggests a blackbody $kT \sim 50$ eV (cf. fig. 8 of Henze et al. 2014a). Using the PIMMS software (v4.8c) we estimated an energy conversion factor (count rate divided by unabsorbed flux in the 0.2–1.0 keV band) of 1.2×10^{10} ct cm^2 erg^{-1} for the XRT (PC mode). We derived the corresponding X-ray luminosities in Table 2 by assuming a distance to IC 1613 of 730 kpc.

2.4 Reddening

IC 1613 is subject to only a small amount of foreground reddening [$E(B-V) = 0.021$; Schlafly & Finkbeiner 2011]. However, estimating the reddening internal to IC 1613 at the position of the nova is difficult, as this is highly variable throughout the galaxy (Garcia et al. 2009). In a survey of IC 1613 Cepheid variables, Pietrzyński et al. (2006) found an average total reddening of $E_{B-V} = 0.090 \pm 0.019$ to the Cepheids, which we take as the extinction estimate for our absolute magnitude calculations.

3 RESULTS

3.1 Photometric evolution

A light curve showing all the photometry taken by the LT, LCO 2 m and *Swift* is shown in Fig. 2. This photometry is also tabulated in the Appendix and presented in the form of spectral energy distributions (SEDs) in Section 3.3. The light curve shows that the nova was clearly discovered prior to peak.

The nova follows a relatively uniform decline, although the r'-band fades significantly slower than B, V and i' due to the increasingly strong influence of the Hα emission line on the broad-band photometry. Initially, the nova also declines more slowly in the

[3] IRAF is distributed by the National Optical Astronomy Observatory, which is operated by the Association of Universities for Research in Astronomy (AURA) under a cooperative agreement with the National Science Foundation.
[4] http://www.swift.ac.uk/user_objects

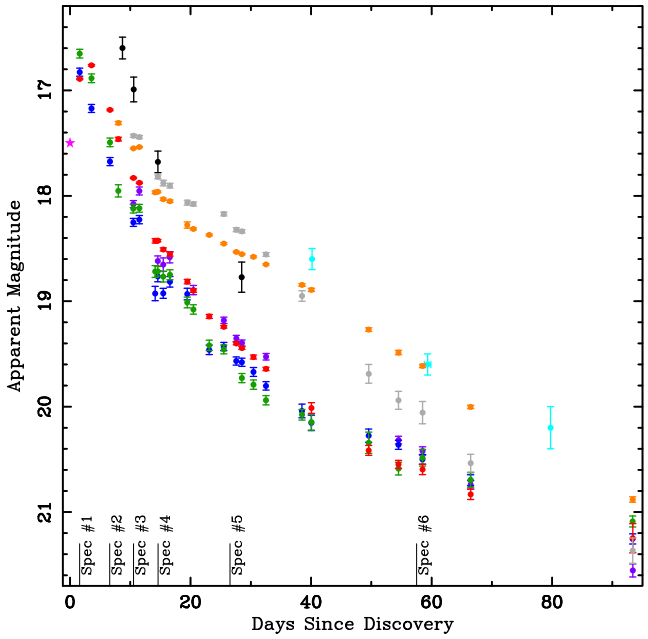

Figure 2. Light curve of Nova IC 1613 2015. The colours represent different filters: *UVW*1, cyan; u', purple; *B*, blue; *V*, green; r', orange; i', red; z', grey; *H*, black. The magenta star shows the unfiltered discovery magnitude. The points on the light curve that correspond to the dates the spectra were taken are also indicated.

z'-band than other filters, but by 40 d post-discovery, the z'-band declines more quickly than the other filters. The initial slow z' decline is unlikely to indicate a change in the overall nova SED, as the (V–i') colour evolution remains relatively unaltered during this phase (the early *H*-band observations are also consistent) and therefore the slower z' decline is probably line driven. As we have no spectra extending beyond 8000 Å, the species that may be responsible for this is not certain, but we suggest it is most likely due to very strong O I 8446 Å emission (caused by Lyβ fluorescence; see discussion in Section 3.2).

Adopting a distance modulus 24.31 ± 0.04 (weighted average from Scowcroft et al. 2013; Menzies et al. 2015) and correcting for reddening using $E(B-V) = 0.090 \pm 0.019$ (Pietrzyński et al. 2006) and the extinction law from Cardelli, Clayton & Mathis (1989, $R_V = 3.1$) gives an absolute magnitude for the eruption peak of $MV = -7.93 \pm 0.08$, which is typical for a nova. The absolute magnitude at 15 d after peak is $MV = -5.84^{+0.20}_{-0.10}$, we note that the (conservative) constraints on the time of peak (assuming 2016 September $12.09^{+1.95}_{-1.61}$ UT) dominate the upper error bar. This is similar to that expected from the relationships of the absolute magnitudes of novae 15 (or 17) d after peak brightness in M49 ($M_{V,15} = -6.36 \pm 0.19$; Ferrarese, Côté & Jordán 2003) and M87 ($M_{F606W,17} = -6.06 \pm 0.23$; Shara et al. 2017, although note that the 'wide *V*' F606W filter contains Hα). We measure the de-reddened day-15 colour, $(B-V)_{t=15} = -0.03^{+0.11}_{-0.14}$. In the SDSS filters, we find $M_{r',15} = -6.50^{+0.17}_{-0.09}$, $(u'-r')_{t=15} = 0.34^{+0.14}_{-0.09}$, $(r'-i')_{t=15} = -0.56 \pm 0.05$ and $(i'-z')_{t=15} = 0.60^{+0.08}_{-0.05}$. The *H*-band coverage is much poorer than the other filters, but using extrapolation we estimate $M_{H,15} = -6.53^{+0.22}_{-0.20}$.

Taking the brightest data point as the peak magnitude of the nova, and using linear extrapolation between the data points, we estimate the t_2 of this nova to be 15 ± 3, 13 ± 2 and 15 ± 3 d in *B*, *V* and i' filters, respectively. We estimate the t_3 values to be $t_{3(B)} = 32 \pm 3$, $t_{3(V)} = 26 \pm 2$ and $t_{3(i')} = 32 \pm 3$ d (the uncertainties here are largely due to the cadence around peak).

3.2 Spectroscopic evolution

Novae have been observed spectroscopically for 150 yr, since the first eruption of RN T Coronae Borealis in 1866 (Huggins 1866). Nova spectra tend to fit into one of the two groups, named after the dominant non-Balmer species in the spectra, Fe II and He/N classes (Williams 1992). These two types of spectra are suggested to form in different components of gas, with the spectral type observed for a given nova reflecting the dominant spectral component at that time (Williams 2012). The Fe II spectra have been suggested to originate in the circumbinary gas originating from the companion star, whereas the He/N type is suggested to be produced by the ejecta themselves (Williams 2012). Although there are some exceptions, Fe II novae tend to produce narrower emission lines than He/N novae (see e.g. Williams 1992; Shafter et al. 2011). Line identification can be difficult in novae due to the broad lines and often differing line profiles. This is further complicated when using low-resolution spectra, which are often required to study faint extragalactic novae. However, the multiple epochs of spectra we have obtained allow us to identify some lines that may not have been possible with a single observation, and more importantly, better interpret the overall evolution. Line identification was also significantly aided by the extensive nova line list from Williams (2012) and multiplet tables from Moore (1945). The spectra are shown in Figs 3, 4 and 5. All spectra are shown in the frame of the observer, but when discussing the identification of spectroscopic features, rest-frame wavelengths are used. The average radial velocity of IC 1613 is $-231.6\,\mathrm{km\,s^{-1}}$, with a velocity dispersion of $10.8\,\mathrm{km\,s^{-1}}$ (Kirby et al. 2014).

3.2.1 *Optically thick 'fireball' stage*

Our first spectrum was taken on 2015 September 12.07, 1.59 d after discovery, and around peak brightness. The main features of this spectrum are the Balmer lines with clear P Cygni absorption profiles. Hα is seen mainly in emission with a small, blue-shifted absorption component. Hβ is seen with significant emission and absorption components, with Hγ and Hδ mainly detected in absorption. This optically thick spectrum is shown in Fig. 3. Fitting a Gaussian to the Hγ absorption profile and taking into account the radial velocity of IC 1613 itself, the absorption minimum implies a velocity of $1200 \pm 200\,\mathrm{km\,s^{-1}}$. Fe II 5169 Å is seen mainly in absorption, with features corresponding to the Fe II (42) triplet at 4924 and 5018 Å also tentatively detected. A few other weak absorption lines are also seen, e.g. one at 4465 Å from Mg II/Fe II.

3.2.2 *Early decline*

The second spectrum, taken 6.59 d after discovery, shows a dramatic change from the $t = 1.59$ d spectrum and clearly shows the nova nature of the transient, indeed this is the spectrum we used to announce that the transient was a nova eruption in Williams & Darnley (2015). This, along with the third, fourth and fifth spectra, taken at $t = 10.54$, 14.61 and 26.55 d, respectively, is shown in Fig. 4. In the second spectrum, the nova now shows strong Balmer emission, although weak P Cygni absorption components are still present. The Fe II (42) triplet, only just detected in the first spectrum

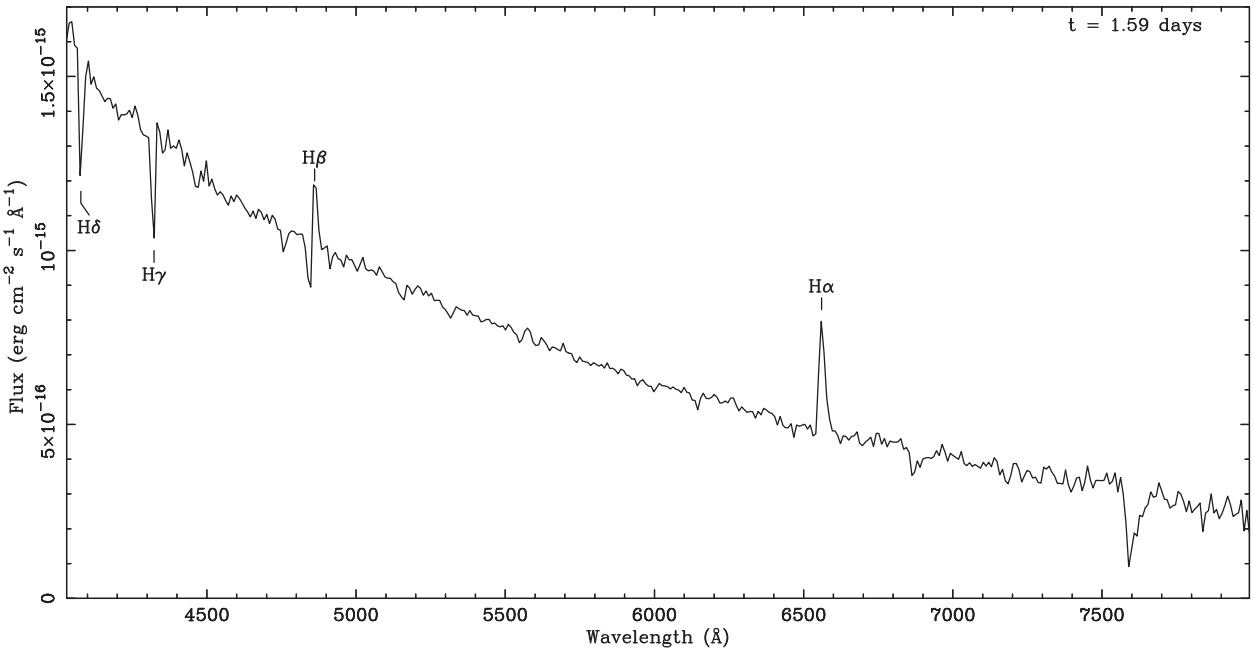

Figure 3. The first spectrum of Nova IC 1613 2015 taken 2015 Sep 12.07 UT, 1.59 d after discovery, and around peak optical brightness.

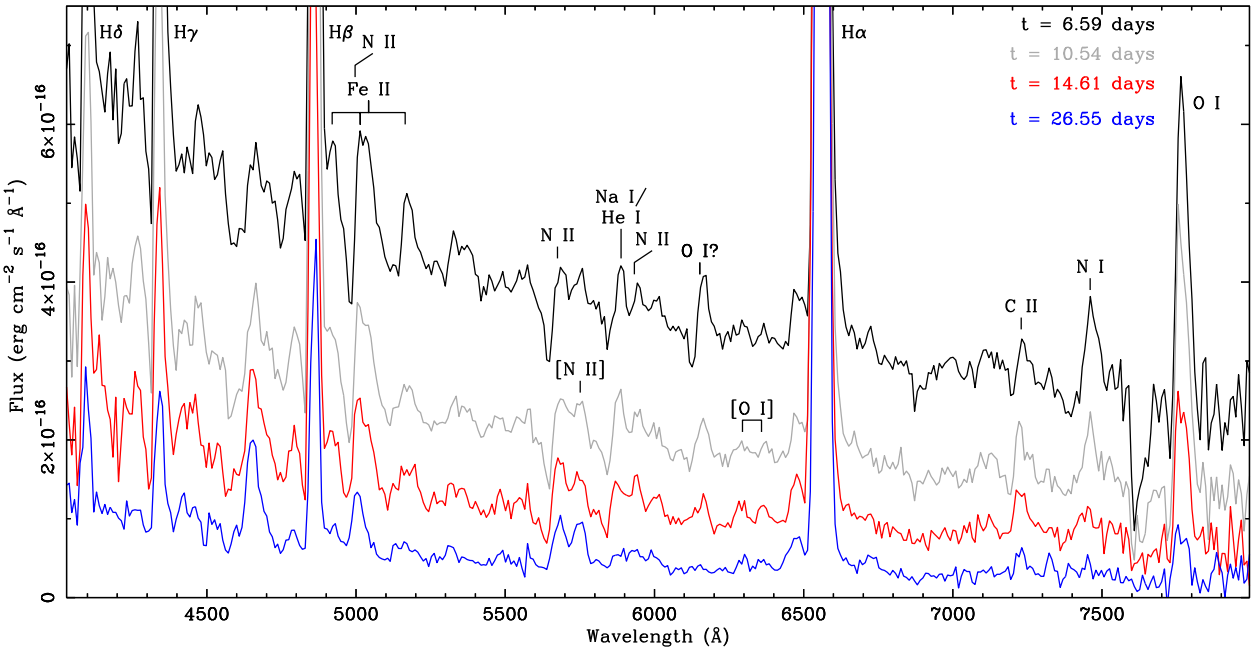

Figure 4. The early decline spectra of Nova IC 1613 2015. These were obtained 2015 September 17.07 UT ($t = 6.59$ d; black line), September 21.02 ($t = 10.54$ d; grey line), September 25.09 ($t = 14.61$ d; red line) and October 7.03 ($t = 26.55$ d; blue line).

is now clearly seen in emission. In the early decline spectra of novae, triplet 42 is typically the strongest of the Fe II lines, although several other multiplets, located between Hα and Hβ, are usually easily identifiable in regular Fe II novae (e.g. 48, 49, 55, and 74). The Fe II (48) multiplet is the only one of these that appears to be weakly detected in Nova IC 1613 2015, with multiplets 49, 55 and 74 not detected.

In the $t = 6.59$ d spectrum, the N I (3) triplet is seen strongly in emission. It also shows a relatively broad absorption component, as would be expected given the wavelengths of the lines that make up the triplet (7424, 7442 and 7468 Å), the velocities associated with the nova and the resolution of the spectrograph. The N II (3) multiplet around 5682 Å is seen with a very strong absorption component, with the N II (28) multiplet at 5938 Å also identified. The profile at the position of the Fe II 5018 Å component of triplet 42, clearly has a different morphology than the 5169 Å line, the former having a strong absorption component. We interpret this as indicating the presence of N II 5001 Å. This is consistent with the morphology of the N II (3) multiplet, which also shows a very strong absorption component. It also explains the evolution of the 5018 Å

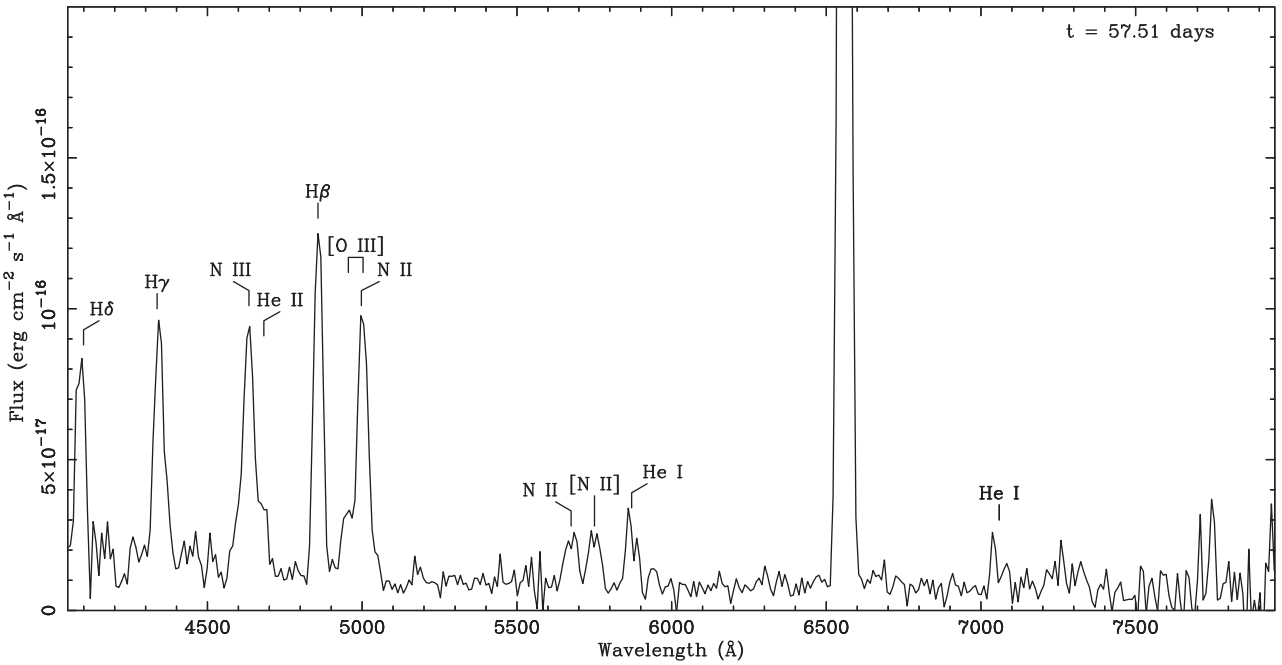

Figure 5. The final spectrum of Nova IC 1613 2015 taken 2015 Nov 6.99 UT, 57.51 d after discovery. This shows the nova in the nebular phase with strong [O III] emission.

line profile between spectra two and five (see below). The Bowen blend (N III/C III/O II; this complex is discussed by Harvey et al. in preparation), which is sometimes referred to as '4640 emission' (it is at ∼4640 Å) is detected as a broad emission line with an accompanying broad absorption profile. This complex is visible at the time of the emergence of the nebular lines in most novae, however is typically only visible in the early spectra if the nova is a member of the He/N spectroscopic class.

The strongest non-Balmer line visible in the $t = 6.59$ d spectrum is O I 7774 Å, produced by O I (1) triplet. There is a relatively strong emission line peaking at 6162 Å (again with an absorption profile). This is clearly not the Fe II (74) multiplet emission line at 6148 Å as the other lines are not present (notably the 6248 Å line, for example). We identify this as most likely being the O I (10) triplet at 6157 Å. Alternatively, it could be N II (which has lines at a similar wavelength), although that is perhaps less likely given it fades to be undetected by the fifth spectrum, which is very different from the other three N II lines (5001, 5682 and 5938 Å), which remain detected even in the final nebular spectrum, as discussed below. In the second spectrum, there is an emission line peaking at 6722 Å. An emission line at this wavelength has been noted since the early days of nova spectroscopy (e.g. DN Geminorum; Wright 1940) and has been suggested as O I 6726 Å (e.g. Baschek 1964, Mason et al. 2005b, Shore et al. 2013, Munari et al. 2014). An alternative explanation would be the N I 6723 Å line.

The Fe II 5018 Å/N II 5001 Å emission line appears to extend further redward than expected from other lines, which indicates the presence of another emission line. There is a He I 5048 Å line which is a possible explanation, but there are no He I lines at 6678 or 7065 Å, so a more likely explanation is N II. In the second and third spectra there is a weak feature at ∼7110 Å, which we identify as C I. We also identify C II emission at 4267 and 7234 Å, which is visible from the day 6.59 to 26.55 spectra.

The spectroscopic evolution between day 6.59 and 26.55 shows the P Cygni profiles, that initially accompany many of the emission lines, weaken over time, as is usually seen in nova eruptions. The Fe II lines weaken along with the N I and O I lines (although O I 7774 Å is still easily visible in the day 26.55 spectrum). The N II and N III lines retain their strength through this evolution and by day 26.55, apart from the Balmer and O I 7774 Å lines, the spectrum is essentially dominated by ionized nitrogen lines (from the point of view of visible features, not the overall flux of the spectrum). The contrasting evolution of the Fe II/N II lines can be seen in the morphology of the blended line due to N II 5001 Å and Fe II 5018 Å, where the blue side of the blend become increasingly dominant as the nova evolves.

3.2.3 Nebular phase

Very few novae beyond the MCs have been observed spectroscopically in the nebular phase. As the evolution progresses, nebular lines also begin to emerge with [O I] (6300 and 6364 Å) clearly detected by day 14.61 and possibly present even earlier. The [O II] 7320/7330 Å doublet is also likely present in the 26.55 d spectrum. Our sixth and final spectrum was taken 57.41 d after discovery and about four magnitudes below peak. This shows further evolution into the nebular phase with [O III] (4959 and 5007 Å) now clearly visible. The 5007/4959 Å emission line ratio is higher than expected (should be ∼3; the lines are highly forbidden and the ratio is essentially fixed), indicating the line is still blended with N II 5001 Å. He II (4686 Å) can now be seen emerging from the Bowen complex, with the peak of the complex itself consistent with it being dominated by N III. We also find He I emission (5876 and 7065 Å). This spectrum is shown in Fig. 5. The emission line fluxes of prominent lines are shown in Table 3.

The assignment of [N II] (5755 Å) is correct in the later spectra (e.g. nebular [N II] would be expected when [O I] is clearly detected in the $t = 14.61$ d spectrum); however, there appears to be a line there even in the $t = 6.59$ d spectrum. This has been noted by other authors (e.g. Iijima & Esenoglu 2003; Surina et al. 2014). There is

Table 3. The evolution of emission line fluxes.

Line identification (rest wavelength)	Emission line flux ($\times 10^{-15}$ erg cm^{-2} s^{-1})					
	$t = 1.59$ d	$t = 6.59$ d	$t = 10.54$ d	$t = 14.61$ d	$t = 26.55$ d	$t = 57.51$ d
Hδ (4102 Å)	–	18.7 ± 3.3	9.5 ± 1.2	7.0 ± 1.9	4.3 ± 1.1	3.9 ± 0.6
Hγ (4341 Å)	–	28.5 ± 5.2	16.6 ± 3.0	9.0 ± 1.6	4.9 ± 0.7	4.4 ± 0.3
Hβ (4861 Å)	3.2 ± 1.6	68.0 ± 4.6	43.9 ± 4.0	24.6 ± 2.9	12.1 ± 1.2	5.4 ± 0.3
Fe II (5169 Å)	–	3.8 ± 0.8	2.7 ± 0.4	2.7 ± 0.6	–	–
N II (5682 Å)	–	1.5 ± 0.5	2.8 ± 0.7	3.2 ± 0.5	3.1 ± 0.3	1.0 ± 0.2
[N II] (5755 Å)	–	1.2 ± 0.2	2.6 ± 0.3	2.5 ± 0.4	3.5 ± 0.3	1.0 ± 0.2
N II (5939 Å)	–	1.1 ± 0.2	2.4 ± 0.6	2.2 ± 0.3	–	–
O I (6157 Å)	–	2.6 ± 0.3	1.8 ± 0.3	1.1 ± 0.3	–	–
[O I] (6300 Å)	–		–	1.0 ± 0.3	0.6 ± 0.2	–
[O I] (6364 Å)	–	–		0.9 ± 0.2	–	–
Hα (6563 Å)	7.3 ± 1.1	146.4 ± 5.1	144.0 ± 5.2	122.0 ± 3.7	90.5 ± 7.4	29.1 ± 2.1
C II (7235 Å)	–	1.4 ± 0.7	2.1 ± 0.7	2.7 ± 0.4	1.2 ± 0.3	–
N I (7452 Å)	–	5.4 ± 0.7	3.2 ± 0.4	1.6 ± 0.5		–
O I (7774 Å)		18.1 ± 2.2	16.6 ± 2.7	8.5 ± 1.7	2.8 ± 1.2	–

Notes. The emission line fluxes are dependent on the assumed continuum level and if a P Cygni absorption component is present, only the emission component of the feature is measured. The fluxes are dereddened for foreground Galactic extinction, assuming $E_{B-V} = 0.021$ and $R_V = 3.1$. The errors do not take into account uncertainties in the flux calibration discussed in Section 2.2.

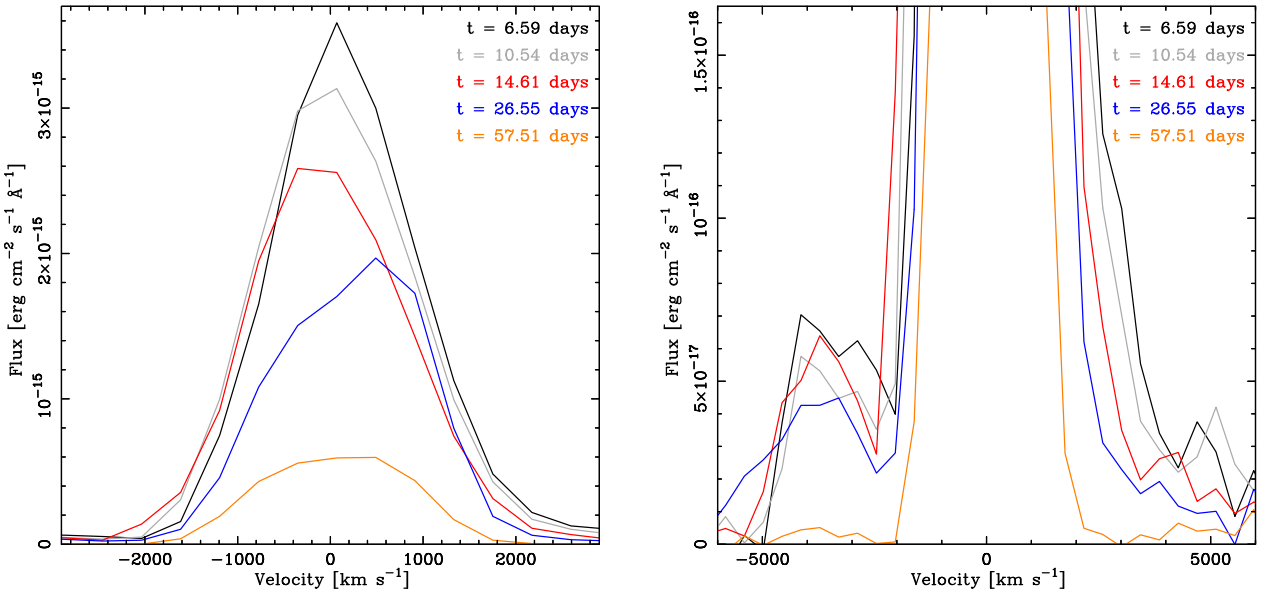

Figure 6. Evolution of the Hα line from $t = 6.59$ to $t = 57.51$ d. The left-hand panel shows the evolution of the shape and absolute flux of the line. The right-hand panel shows the evolution of the fainter emission either side of the main Hα profile (see discussion in Section 3.2.4). The velocities have been corrected for the radial velocity of IC 1613 itself.

also a non-forbidden N II doublet (9) at a very similar wavelength. This is caused by the same excited state as the N II (3) multiplet, but here the electrons transition to $2s^2 2p3s\ ^1P^\circ$, rather than $2s^2 2p3s\ ^3P^\circ$. It is possible that this at least partially contributes to this emission line.

3.2.4 Balmer evolution

By fitting of a Gaussian profile to the emission component of the Hα line in the second ($t = 6.59$ d) spectrum, we measure the full width at half-maximum (FWHM) to be 1580 ± 70 km s^{-1} after correcting for the spectral resolution. The line then apparently broadens to a FWHM of 1750 ± 50 km s^{-1} in the third ($t = 10.54$ d) spectrum and thereafter remains consistent. We measure it at 1760 ± 90, 1750 ± 120 and 1720 ± 190 km s^{-1} in the $t = 14.61$, $t = 26.55$ and $t = 57.51$ d spectra, respectively. The most likely explanation for the early change in the FWHM is that in the $t = 6.59$ d spectrum the Hα emission line is significantly influenced by a P Cygni absorption component, which has the effect of narrowing the apparent emission line.

The peaks of the Balmer emission are not shown in Figs 4 and 5 to allow the reader to view the fainter lines in greater detail. The evolution of the Hα line is show in Fig. 6. The left-hand panel of Fig. 6 shows that the overall profile is relatively symmetrical, with a Gaussian profile generally fitting the central profile well. The only stage when a Gaussian does not appear a good fit is the $t = 26.65$ d spectrum, when the profile seems asymmetric, being stronger at the red side of the profile. Close inspection of the Hα profile in the right-hand panel of Fig. 6 shows that there is emission peaking at around -4000 km s^{-1} (∼6480 Å). Comparing it to the

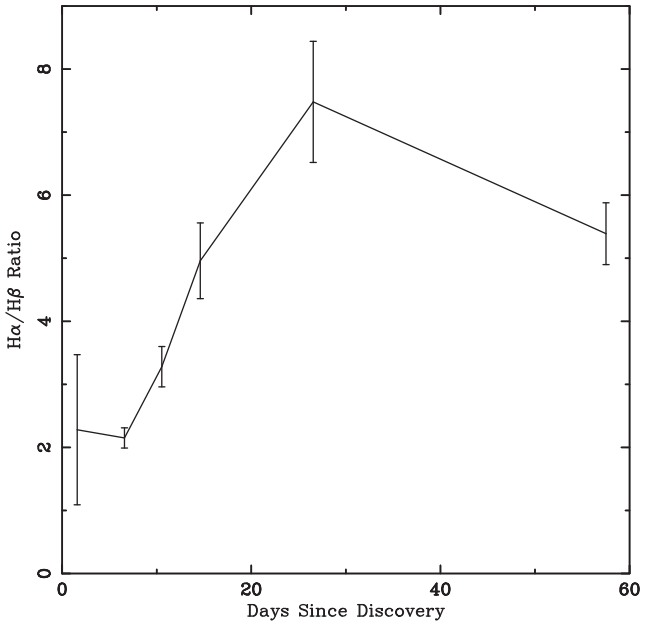

Figure 7. The evolution of the Hα/Hβ intensity ratio between the $t = 6.59$ and $t = 57.51$ d spectra. The ratios are corrected for foreground Galactic reddening ($E_{B-V} = 0.021$).

red side of the Hα line shows that it is too blue to be explained as part of a simple Gaussian with a P Cygni profile superimposed on the emission component, and could be due to emission from N I or N II. An alternative explanation could be a separate higher velocity component to the Hα line as there may be excess flux on the red side of the profile as well, although this ~6480 Å emission appears to persist longer, visible in all but the final nebular spectrum.

In Fig. 7, we show the evolution of the Hα/Hβ ratio between $t = 6.59$ and $t = 57.51$ d, corrected for Galactic reddening ($E_{B-V} = 0.021$). The figure shows that the ratio initially increases, peaking at 7.5 ± 1.0 on $t = 26.55$ d, before declining in the final nebular phase spectrum. During this period, the Hγ/Hβ ratio does not change dramatically. The evolution in the Hα/Hβ ratio can clearly not be caused by dust as such a dramatic change would be seen as a dip in the optical light curve. This Hα/Hβ ratio evolution is common in novae and has been discussed by a number of authors (e.g. Kogure 1961; Meinel 1963; Ferland 1978; Ferland, Shields & Netzer 1979; Anupama et al. 1992; Iijima & Esenoglu 2003). The changing Balmer decrement is caused by self-absorption. If Lyα and Hα have high optical depth, high Hα/Hβ ratios such as those observed here can be produced (Netzer 1975). The calculations made by Netzer (1975) also indicate the Hγ/Hβ ratio does not necessarily change dramatically during this Hα/Hβ evolution, although this is dependent on the Lyα optical depth. This Balmer line ratio behaviour appears to well replicate that observed in Nova IC 1613 2015. In the case of novae in eruption, Case B recombination is not valid (as discussed above), therefore the Balmer decrement cannot, and should not, be used to estimate reddening.

As suggested by Bowen (1947), the close proximity of O I 1025.76 Å to Lyβ (1025.72 Å) can lead to excitation of the O I ground state. This then produces strong emission at the 1.1287 μm and 8446 Å wavelengths as the electrons fall back to the O I ground state (see also Kastner & Bhatia 1995). This effect and its relationship to the Balmer decrement has also been discussed in the context of Seyfert galaxies (Shields 1974). Such Lyβ florescence can only occur under conditions of optically thick hydrogen. The Hα/Hβ ratio and the O I 8446 Å intensity are closely linked (Ferland & Netzer 1979; Ferland et al. 1979), with the Hα/Hβ and (O I 8446 Å)/Hβ line ratios often peaking at a similar point of the eruption (see e.g. Ferland, Lambert & Woodman 1986). We note that between the 26.55 and 57.51 d spectra, the Hα/Hβ ratio drops. Between the 26.55 and 57.51 d spectra, it can also be seen from Fig. 2 that the z'-band fades more rapidly than any other waveband, indicating Lyβ florescence (or specifically the 8446 Å line; as indicated by the drop in the Hα/Hβ ratio) may be the cause of the initially slower z'-band decline mentioned in Section 3.1.

3.3 Spectral energy distributions

SEDs can be derived from multiband photometry or spectra, both of which have drawbacks. Spectra are more time-expensive and are more prone to (variable and colour-dependent) calibration issues. However, they allow prominent spectral features not associated with the underlying SED to be removed before fitting, which broad-band photometric observations do not. This is particularly important in novae, where during an eruption, the broad-band photometry becomes increasingly influenced by line emission and can even be dominated by it at late times (e.g. [O III] and Hα).

Fitting a power-law to the first spectrum (excluding prominent emission and absorption features) indicates at 1.59 d post-discovery, $f_\lambda \propto \lambda^{-2.42\pm0.08}$ at optical wavelengths. This is near that expected from optically thick free–free emission ($f_\lambda \propto \lambda^{-8/3}$; Wright & Barlow 1975). The relatively short wavelength coverage however is also consistent with a blackbody. Fitting a blackbody function to the first spectrum yields a photospheric temperature of 11600 ± 500 K. This is close to the expected effective temperature of a nova at peak (~8000 K; see e.g. Prialnik 1986; Beck et al. 1995; Evans et al. 2005). 5 d later the wavelength dependence of the optical continuum had changed dramatically to $f_\lambda \propto \lambda^{-1.48\pm0.08}$, even shallower than that expected from optically thin free–free ($f_\lambda \propto \lambda^{-1.9}$). The measured wavelength dependence of the SED increases for the third (10.54 d) spectrum, with $f_\lambda \propto \lambda^{-1.58\pm0.09}$, although note that these are consistent within the errors. The other three spectra give $\propto \lambda^{-1.68\pm0.11}$, $\propto \lambda^{-2.11\pm0.12}$ and $\propto \lambda^{-1.21\pm0.18}$ on days 14.61, 26.55 and 57.51, respectively. Note that these fits only include the known foreground reddening ($E_{B-V} = 0.021$), therefore the intrinsic slope of the SEDs of the nova eruption could be bluer.

The SEDs from the multiband photometry are shown in Fig. 8. The photometry taken at similar epochs as the spectra discussed above are broadly consistent with the power laws derived from the spectra themselves, keeping in mind that as the nova fades, the broad-band photometry becomes increasingly influenced by strong emission lines (e.g. Balmer and O I, and later [O III]). The photometry undoubtedly confirms that the dramatic change in the slope of the optical continuum emission between the spectra on day 1.59 and day 6.59 is real. Indeed a large change occurs between day 1.6 (i.e. the time of the first spectrum) and day 3.6.

3.4 X-rays

We do not detect X-ray emission from the nova between days 40 and 330 after eruption. The resulting luminosity upper limits, listed in Table 2 for each individual *Swift* observation, were typically below 5×10^{37} erg s^{-1}. This allows us to rule out a bright SSS under the conservative assumption of a 50 eV blackbody spectrum (the fastest novae are considerably hotter, see e.g. Osborne et al. 2011; Henze et al. 2014b; Page et al. 2015). Before day 40, the nova was still

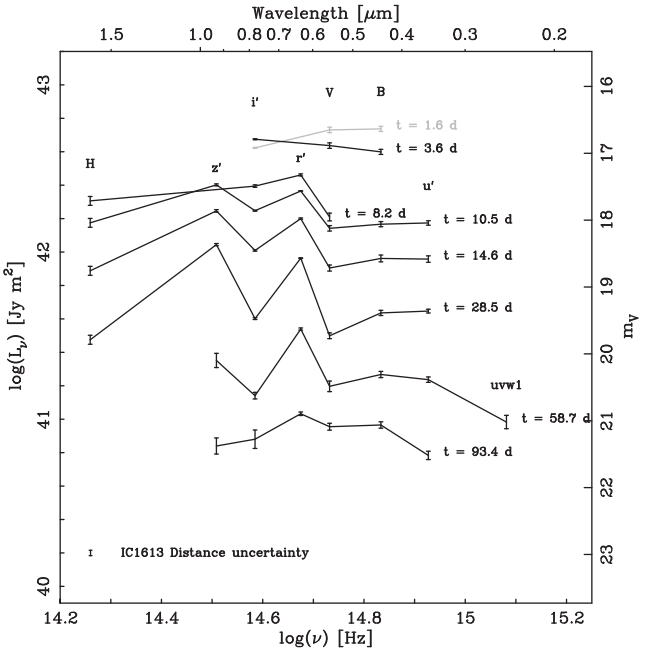

Figure 8. SEDs of Nova IC 1613 2015 from peak to 93.4 d post-discovery (around $m_V = 4.4$ below peak). The extreme effect of the Hα emission on the r'-band photometry can easily be seen. The size of the systematic uncertainty from the distance of IC 1613 is indicated near the bottom of the plot.

bright in UV and no X-rays would have been emitted (cf. Henze et al. 2015). An observing gap between days 160 and 260 (Table 2) is likely too short to hide an SSS phase: based on our experience with the M31 population, a nova with an SSS turn-on time of more than 160 d would be expected to be visible in X-rays for longer than 260 d (Henze et al. 2014a).

Combining all observations in Table 2 (32.6 ks) we derive an upper limit of 4.5×10^{-4} ct s^{-1}, corresponding to a luminosity of 2.4×10^{35} erg s^{-1}. This is an order of magnitude lower than the observed luminosities of faint novae in M31 (Henze et al. 2010, 2011, 2014a). Since fainter novae are typically visible for longer (Henze et al. 2014a), we can rule out a low-luminosity SSS counterpart for the observed time range. Note that this upper limit would only be valid if such a low-luminosity SSS was emitting over the whole time frame of the *Swift* observations.

3.5 The progenitor search

The position of Nova IC 1613 2015 is not covered by *Hubble Space Telescope* data (which is ideal for such progenitor searches due to its high resolving power and large wavelength coverage), however at the distance of IC 1613, the most luminous quiescent systems will still be detectable in deep ground-based data. As we noted in Williams & Darnley (2015), the nova appears very close to a $V = 22.06$, $I = 21.53$ magnitude source recorded at $01^h04^m43^s.56$ $+02°03'42''.0$ (J2000) in Udalski et al. (2001).

The field was observed with the Very Large Telescope (VLT) using the FOcal Reducer/low dispersion Spectrograph 2 (FORS2; Appenzeller et al. 1998) on 2012 August 20 under proposal 090.D-0009(A) and using the R_SPECIAL filter (effective wavelength 6550 Å). Using the method described in detail by Bode et al. (2009), Darnley et al. (2014) and Williams et al. (2014), we used reference stars in r'-band LT eruption images to precisely determine the position of the nova in the archival data. This is shown in Fig. 9. We also independently (using different reference stars) calculated the position of the nova in archival SDSS g-band OmegaCAM (Kuijken et al. 2002; Kuijken 2011) data taken at the 2.6 m VLT Survey Telescope (Arnaboldi et al. 1998) on 2014 December 17, using V-band LT data.

In the first archival image where the position was derived from the r'-band LT eruption observations, the position of the nova is calculated to be $0''.09 \pm 0''.05$ south and $0''.21 \pm 0''.05$ east of the progenitor candidate. Using the errors on the positional transformation and the centroid on the nova/stellar source implies an association between the two sources can be ruled out at the 4.1σ level. In the second image, we calculate the position of the nova to be $0''.05 \pm 0''.05$ north and $0''.25 \pm 0''.05$ east. From this it appears the progenitor candidate may have a small, but real offset (eastward) from the nova.

As a check for a systematic offset across the transformed field, we apply the positional transformation to 10 stars in close proximity to the nova (within $\sim 1'$), that were not used in the calculation of the positional transformation itself. There is no evidence for a systematic offset in these sources, with the average x/y offsets less than the standard deviation in the offsets. The standard deviation of these offsets however does indicate that it is possible that the errors on the transformation are slightly underestimated. We therefore apply the average x/y offsets (in the R_SPECIAL image) to the position of the nova. Using the standard deviation as the error indicates an association is still ruled out, but with a reduced 3σ confidence. It is also worth noting that the transformed position of the source to the south-east of the nova (the brightest star seen in the left-hand panel of Fig. 9) is consistent within 1.1σ (using the errors of the transformation itself) of that of the centroided position from the VLT image. If there were a systematic offset affecting the nova transformation, one would expect it to also be present in this very nearby ($\sim 5''$ separation) source.

We therefore conclude that, despite the close proximity of the progenitor candidate, it is most likely simply a chance alignment. However, this should be confirmed by late-time spectroscopy. Novae retain strong Balmer emission for a significant time after eruption, but over time the optical spectrum becomes increasingly dominated by [O III] emission lines. If this progenitor candidate is indeed the luminous accretion disc of the pre-eruption nova, a quiescent spectrum may be expected to reveal narrow Balmer and He II emission. The lack of (broader) [O III] lines would confirm we are not observing an extended tail of the nova eruption.

4 DISCUSSION

A comparison of Nova IC 1613 2015 with other IC 1613 novae is not possible due to the lack of data for the 1954 and 1996 candidates. We can however compare it to other extragalactic novae residing in Local Group galaxies.

At $t_{2(V)} = 13 \pm 2$ d, Nova IC 1613 2015 can be considered a fast-fading nova (Gaposchkin 1957). Comparing it to the cumulative t_2 distribution plot of M31 novae from Williams et al. (2016) would place it in the fastest 20 per cent of novae. However, a better comparison may be the LMC, and comparing the t_2 value to those in Table 2 from Shafter (2013) reveals that in this (albeit small) sample, novae significantly slower than Nova IC 1613 2015 are relatively rare. The low nova rate of the SMC, perhaps the best comparison to IC 1613, makes a comparison to the overall SMC population difficult. There are several SMC novae with good light curves (see e.g. Henize, Hoffleit & McKibben Nail 1954; de Laverny et al. 1998;

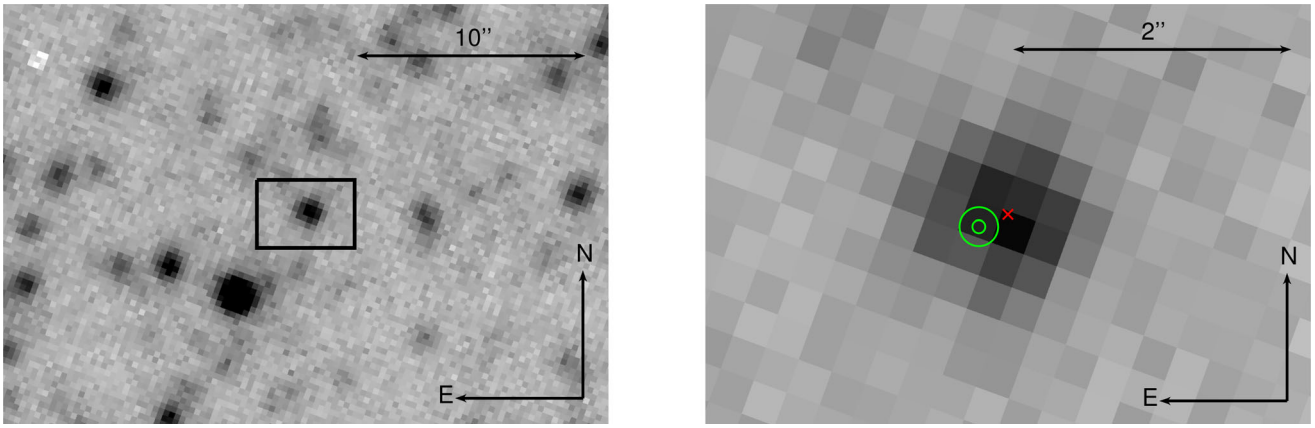

Figure 9. The position of the nova in pre-eruption data compared to the nearby resolved source. Left: the Nova IC 1613 2015 nova field imaged with FORS2 on the VLT using an R_SPECIAL filter on 2012 August 20. The black box indicates the zoomed in region shown in the right-hand panel. Right: the same data as the left-hand panel, with the 1σ and 3σ errors on the position of the nova (calculated from r'-band LT eruption data) indicated by green circles and the position of the nearby resolved source indicated by a red '×'.

Mróz et al. 2016) which display a broad range of decline times, and Nova IC 2016 2015 would certainly not seem out of place amongst these. Indeed, there have been some novae that evolved much more slowly than Nova IC 1613 2015 (e.g. Nova SMC 1994, de Laverny et al. 1998; Nova SMC 2001, Liller, Shida & Jones 2004; Mróz et al. 2016).

The early decline spectra of Nova IC 1613 2015 are not typical of novae. In M31, around 80 per cent of all novae belong to the Fe II class (Shafter et al. 2011). From the smaller sample size of LMC and M33 novae, a lower proportion (perhaps around 50 per cent) appear to be Fe II novae in these galaxies (Shafter et al. 2012; Shafter 2013). The hybrid spectroscopic class of novae can either evolve from one type to another or show both types simultaneously. Nova IC 1613 2015 shows both Fe II lines and N II in the early decline spectra, classifying it as a hybrid nova. It is worth noting that it is not unreasonable to expect hybrid novae that transition from one type to another to go through a phase which simultaneously shows both types, even if it is only short lived. The early decline spectral evolution shows many similarities to the hybrid Nova LMC 1988 No. 2 (see Sekiguchi et al. 1989 and Williams et al. 1991), although Nova IC 1613 2015 fades significantly more slowly, with Nova LMC 1988 No. 2 having a t_2 of around 5 d (Sekiguchi et al. 1989). The evolution of Nova IC 1613 2015 also appears similar to the Galactic nova V5114 Sagittarii, which had a similar t_2 (∼11 d) and showed somewhat similar spectroscopic evolution and associated velocities (Hα FWHM ∼2000 km s^{-1}; Ederoclite et al. 2006), although in this case the spectrum shortly after peak appears closer to a typical Fe II nova (Ederoclite et al. 2006) than Nova IC 1613 2015.

As the best Local Group galaxy with observed novae to compare IC 1613 to is the SMC, it is worth reviewing the spectroscopic information on SMC novae. Nova SMC 1951 was observed spectroscopically several times and clearly shows the Bowen blend emission complex (Henize et al. 1954). However, most novae show this at later times, so an unambiguous spectroscopic type cannot be assigned. Nova SMC 1952 was observed 2 d after peak and likely showed He I and He II emission (Smith 1954), classifying it as an He/N nova. Nova SMC 2001 was an Fe II nova (Mason et al. 2005b). Nova SMC 2005 shows broad Fe II lines (Mason et al. 2005a), so is classed as an Fe IIb nova. Most recently, the first spectrum taken of Nova SMC 2016 was consistent with it being a member of the He/N spectroscopic class (Williams & Darnley 2016). We note that Nova SMC 2016 has extensive pan-chromatic coverage (see e.g. Darnley & Williams 2016; Kuin et al. 2016; Orio et al. 2016; Page et al. 2016), which will be seen in forthcoming publication(s). The lack of early decline spectra of SMC novae prevents any conclusions being made on the proportion of novae that are Fe II novae or how Nova IC 1613 2015 compares to the SMC population.

There are clearly significant changes in the wavelength dependence of the underlying continuum in the early stages of the eruption, which is apparent from the spectra, where the slope of the continuum changes from $f_\lambda \propto \lambda^{-2.42\pm0.08}$ 1.59 d after discovery to $f_\lambda \propto \lambda^{-1.48\pm0.08}$ 6.59 d after eruption. This is supported by the photometry where the nova shows a much redder colour 3.6 d after discovery compared to 1.6 d after discovery. In a nova eruption the B, V and i'' magnitudes are not greatly affected by line emission until the latter stages.

If we ignore the first two photometry points (where we have already established the continuum has changed dramatically over a short time), the B, V and i' light curves are relatively well described by a power law. We find $f_{B(\lambda)} \propto t^{-1.22}$, $f_{V(\lambda)} \propto t^{-1.28}$ and $f_{i'(\lambda)} \propto t^{-1.46}$ (where t is days since discovery), which indicates the nova is becoming increasingly blue as the eruption evolves (as seen between spectra 2 and 5). However, examining the $(B-V)$ colour evolution shows the picture is slightly more complex. The $(B-V)$ colour becomes lower until $m_V \sim 20$ (around day 30−40) and then turns around and $(B-V)$ begins increasing (getting redder). This behaviour is seen in other novae (see for example fig. 39 in Hachisu & Kato 2014 and fig. 7 in Darnley et al. 2016). While this seems in general agreement with the power law of the final spectrum becoming shallower, we also must note that while B and V magnitudes are not as influenced by line emission early in the eruption, during the nebular phase, lines such as [O III] become increasingly dominant (and thus affect the broad-band colours, but are removed from the power-law fitting in Section 3.3).

The X-ray upper limits in Table 2 indicate that either the SSS phase had not started yet before day 330 or that the nova did not become visible in soft X-rays at all. If this were a M31 nova, then the fast t_2 and reasonably high expansion velocity would (consistently) predict an SSS turn-on time of about 50–90 d for a subset with similar properties (cf. Henze et al. 2014a). This is in agreement with the optical spectra indicating that by day 57 the nova had entered its nebular phase, where the ejecta would have become optically thin

to X-rays. However, note that only a fraction of novae in the M31 reference sample showed SSS emission, which cannot be explained by observational coverage alone (Henze et al. 2011, 2014a).

If we assume that by day 57 the nuclear burning in the residual hydrogen envelope (i.e. the part that was not ejected) had already extinguished, then we can estimate an upper limit on the mass of this envelope. Following the approach described in Henze et al. (2014a, see also the relevant references therein) an SSS turn-off time of 57 d would correspond to a burned mass of 2.7×10^{-7} $M_{\odot}$. Such relatively low masses are rare, but have been estimated for a few fast novae from the M31 sample (Henze et al. 2014a). However, we stress the fact that for an individual object a large variety of factors, such as eruption geometry or inclination angle, can play a role in obscuring an existing SSS emission component.

Furthermore, there will of course be systematic differences between the nova samples of IC 1613 and M31, the latter of which we have learnt a great deal about nova population properties from. Different metallicities have been found to affect the average nova properties: see for instance the comparisons of M31 and LMC novae by della Valle & Duerbeck (1993); Shafter (2013) and the theoretical models of (Hachisu & Kato 2006; Kato, Hachisu & Henze 2013). It remains unclear whether these systematics are large enough to affect the SSS phase of the nova significantly (e.g. to confine it to the narrow gap between days 160 and 260). Without further evidence we could only speculate on the specific causes for the SSS non detection, and we refrain from doing so.

5 SUMMARY AND CONCLUSIONS

We have presented detailed photometric and spectroscopic observations of the Nova IC 1613 2015 eruption, from the early optically thick stage, through the early decline and nebular phases. This is the first detailed study of a nova residing in an irregular dwarf galaxy beyond the much closer MCs. Here, we summarize our observations and conclusions:

(i) We have undertaken a detailed observing campaign of Nova IC 1613 2015, with ground-based photometry and spectroscopy led by the LT, with further observations from LCO. We also obtained UV photometry and X-ray observations with *Swift*.

(ii) The light curve shows a relatively smooth decline and the nova is classified as a fast nova, with $t_{2(V)} = 13 \pm 2$ and $t_{3(V)} = 26 \pm 2$ d. The absolute peak magnitude of the nova is $MV = -7.93 \pm 0.08$, which is typical for a classical nova.

(iii) The X-ray observations taken between 40 and 330 d after discovery detected no SSS emission associated with the nova.

(iv) The spectra show that the nova is a member of the 'hybrid' spectroscopic class, with it initially showing relatively strong Fe II lines and comparable N II lines. By the time it had declined by two magnitudes, the N II/N III features are significantly stronger than Fe II.

(v) One of the more unusual features is a strong emission line peaking at ∼6162 Å. We interpret this as likely due to O I (6157 Å), or possibly N II.

(vi) The FWHM of the Hα emission line is measured at around 1750 km s^{-1} and shows relatively little change over the course of the eruption.

(vii) The Hα/Hβ ratio initially increases through the early decline spectra (due to self-absorption; peaking at 7.5 ± 1.0), before declining in the nebular spectrum. This implies the z'-band light curve may be significantly influenced by a strong O I 8446 Å emission line, which in turn is caused by Lyβ fluorescence.

(viii) We also obtained a nebular spectrum of Nova IC 1613 2015, with [N II], [O I], [O II] and [O III] all detected. This makes it one of the first novae beyond the MCs to be observed in the nebular phase.

(ix) The first spectrum taken around peak shows a steep blue continuum of $f_{\lambda} \propto \lambda^{-2.42 \pm 0.08}$, similar to that expected from optically thick free–free emission, but also consistent with photospheric (blackbody) emission. The second spectrum shows a dramatic change in the continuum to $f_{\lambda} \propto \lambda^{-1.48 \pm 0.08}$. A sudden change in the underlying continuum between the two epochs is supported by the photometry.

(x) Despite the very close proximity of the nova to a stellar source, we find that this is most likely a chance alignment.

To further our understanding of how nova eruptions depend on the underlying stellar population it is important that we take the opportunity to study novae occurring in significantly different environments than can be found in the usual targets of M31 and our own Galaxy.

ACKNOWLEDGEMENTS

We would like to thank the referee, Mike Shara, whose suggestions helped improve this paper. SCW acknowledges a visiting research fellowship at Liverpool John Moores University (LJMU). MH acknowledges the support of the Spanish Ministry of Economy and Competitiveness (MINECO) under the grant FDPI-2013-16933 as well as the support of the Generalitat de Catalunya/CERCA programme. The Liverpool Telescope is operated on the island of La Palma by LJMU in the Spanish Observatorio del Roque de los Muchachos of the Instituto de Astrofisica de Canarias with financial support from the UK Science and Technology Facilities Council. This work makes use of observations from the LCO network. This work made use of data supplied by the UK *Swift* Science Data Centre at the University of Leicester. Based in part on data obtained from the ESO Science Archive Facility under request numbers scw233242 and scw233245.

REFERENCES

Ahn C. P. et al., 2012, ApJS, 203, 21
Anupama G. C., Duerbeck H. W., Prabhu T. P., Jain S. K., 1992, A&A, 263, 87
Appenzeller I. et al., 1998, Messenger, 94, 1
Arnaboldi M., Capaccioli M., Mancini D., Rafanelli P., Scaramella R., Sedmak G., Vettolani G. P., 1998, Messenger, 93, 30
Arnould M., Norgaard H., 1975, A&A, 42, 55
Barnsley R. M., Jermak H. E., Steele I. A., Smith R. J., Bates S. D., Mottram C. J., 2016, J. Astron. Telesc. Instrum. Syst., 2, 015002
Baschek B., 1964, PASP, 76, 22
Beck H. K. B., Hauschildt P. H., Gail H.-P., Sedlmayr E., 1995, A&A, 294, 195
Bode M. F., Evans A., 2008, Classical Novae 2nd edn. Cambridge Univ. Press, Cambridge
Bode M. F., Darnley M. J., Shafter A. W., Page K. L., Smirnova O., Anupama G. C., Hilton T., 2009, ApJ, 705, 1056
Bouret J.-C., Lanz T., Hillier D. J., Martins F., Marcolino W. L. F., Depagne E., 2015, MNRAS, 449, 1545
Bowen I. S., 1947, PASP, 59, 196
Brown T. M. et al., 2013, PASP, 125, 1031
Burrows D. N. et al., 2005, Space Sci. Rev., 120, 165
Cardelli J. A., Clayton G. C., Mathis J. S., 1989, ApJ, 345, 245
Darnley M. J., Williams S. C., 2016, Astron. Telegram, 9688
Darnley M. J. et al., 2006, MNRAS, 369, 257
Darnley M. J., Ribeiro V. A. R. M., Bode M. F., Hounsell R. A., Williams R. P., 2012, ApJ, 746, 61

Darnley M. J., Williams S. C., Bode M. F., Henze M., Ness J.-U., Shafter A. W., Hornoch K., Votruba V., 2014, A&A, 563, L9
Darnley M. J. et al., 2016, ApJ, 833, 149
de Laverny P. et al., 1998, A&A, 335, L93
della Valle M., Duerbeck H. W., 1993, A&A, 271, 175
Dickey J. M., Lockman F. J., 1990, ARA&A, 28, 215
Ederoclite A. et al., 2006, A&A, 459, 875
Evans A., Tyne V. H., Smith O., Geballe T. R., Rawlings J. M. C., Eyres S. P. S., 2005, MNRAS, 360, 1483
Evans P. A. et al., 2009, MNRAS, 397, 1177
Ferland G. J., 1978, ApJ, 219, 589
Ferland G., Netzer H., 1979, ApJ, 229, 274
Ferland G. J., Shields G. A., Netzer H., 1979, ApJ, 232, 382
Ferland G. J., Lambert D. L., Woodman J. H., 1986, ApJS, 60, 375
Ferrarese L., Côté P., Jordán A., 2003, ApJ, 599, 1302
Filippenko A. V., Li W. D., Treffers R. R., Modjaz M., 2001, in Paczynski B., Chen W.-P., Lemme C., eds, ASP Conf. Ser. Vol. 246, IAU Colloq. 183: Small Telescope Astronomy on Global Scales. Astron. Soc. Pac., San Francisco, p. 121
Gaposchkin C. H. P., 1957, The Galactic Novae, Amsterdam, North-Holland. Wiley-Interscience, New York
Garcia M., Herrero A., Vicente B., Castro N., Corral L. J., Rosenberg A., Monelli M., 2009, A&A, 502, 1015
Garcia M., Herrero A., Najarro F., Lennon D. J., Alejandro Urbaneja M., 2014, ApJ, 788, 64
Gehrels N. et al., 2004, ApJ, 611, 1005
Hachisu I., Kato M., 2006, ApJS, 167, 59
Hachisu I., Kato M., 2014, ApJ, 785, 97
Halevi G., Zheng W., Filippenko A. V., 2015, Central Bureau Electronic Telegrams, 4186, 1
Henize K. G., Hoffleit D., McKibben Nail V., 1954, Proc. Natl. Acad. Sci., 40, 365
Henze M. et al., 2010, A&A, 523, A89
Henze M. et al., 2011, A&A, 533, A52
Henze M. et al., 2014a, A&A, 563, A2
Henze M., Ness J.-U., Darnley M. J., Bode M. F., Williams S. C., Shafter A. W., Kato M., Hachisu I., 2014b, A&A, 563, L8
Henze M. et al., 2015, A&A, 580, A46
Hernanz M., Jose J., Coc A., Isern J., 1996, ApJ, 465, L27
Hillebrandt W., Niemeyer J. C., 2000, ARA&A, 38, 191
Hillman Y., Prialnik D., Kovetz A., Shara M. M., 2016, ApJ, 819, 168
Hoyle F., Fowler W. A., 1960, ApJ, 132, 565
Huggins W., 1866, MNRAS, 26, 275
Iijima T., Esenoglu H. H., 2003, A&A, 404, 997
Izzo L. et al., 2015, ApJ, 808, L14
Jordi K., Grebel E. K., Ammon K., 2006, A&A, 460, 339
Kastner S. O., Bhatia A. K., 1995, ApJ, 439, 346
Kato M., Hachisu I., Henze M., 2013, ApJ, 779, 19
King J. Y., Modjaz M., Li W. D., 1999, IAU Circ., 7287, 2
Kirby E. N., Bullock J. S., Boylan-Kolchin M., Kaplinghat M., Cohen J. G., 2014, MNRAS, 439, 1015
Kogure T., 1961, PASJ, 13, 335
Kraft R. P., 1964, ApJ, 139, 457
Kraft R. P., Burrows D. N., Nousek J. A., 1991, ApJ, 374, 344
Krautter J., Oegelman H., Starrfield S., Wichmann R., Pfeffermann E., 1996, ApJ, 456, 788
Kuijken K., 2011, Messenger, 146, 8
Kuijken K. et al., 2002, Messenger, 110, 15
Kuin N. P. M., Page K. L., Williams S. C., Darnley M. J., Shore S. N., Walter F. M., 2016, Astron. Telegram, 9635
Kurtev R., Georgiev L., Borissova J., Li W. D., Filippenko A. V., Treffers R. R., 2001, A&A, 378, 449
Liller W., Shida R. Y., Jones A. F., 2004, Inf. Bull. Var. Stars, 5582
Mantegazza L., Antonello E., Fugazza D., Bossi M., Covino S., 2001, A&A, 367, 759
Maoz D., Mannucci F., Nelemans G., 2014, ARA&A, 52, 107
Mason E., Brandeker A., Ederoclite A., Della Valle M., 2005a, Central Bureau Electronic Telegrams, 195
Mason E., Della Valle M., Gilmozzi R., Lo Curto G., Williams R. E., 2005b, A&A, 435, 1031
Meinel A. B., 1963, ApJ, 137, 834
Menzies J. W., Whitelock P. A., Feast M. W., 2015, MNRAS, 452, 910
Molaro P., Izzo L., Mason E., Bonifacio P., Della Valle M., 2016, MNRAS, 463, L117
Moore C. E., 1945, Contributions from the Princeton University Observatory, 20, 1
Mróz P. et al., 2016, ApJS, 222, 9
Munari U. et al., 2014, MNRAS, 440, 3402
Neill J. D., Shara M. M., 2004, AJ, 127, 816
Netzer H., 1975, MNRAS, 171, 395
Nomoto K., Thielemann F.-K., Yokoi K., 1984, ApJ, 286, 644
Nugent P. E. et al., 2011, Nature, 480, 344
Oke J. B., 1990, AJ, 99, 1621
Orio M., Behar E., Rauch T., Zemk P., 2016, The Astronomer's Telegram, 9810
Osborne J. P. et al., 2011, ApJ, 727, 124
Page K. L. et al., 2015, MNRAS, 454, 3108
Page K., Osborne J., Kuin P., Shore S., Williams S., Darnley M. J., 2016, Astron. Telegram, 9733
Piascik A. S., Steele I. A., Bates S. D., Mottram C. J., Smith R. J., Barnsley R. M., Bolton B., 2014, in Ramsay S. K., McLean I. S., Takami H., eds, Ground-based and Airborne Instrumentation for Astronomy V. SPIE, Bellingham, p. 8
Pietrzyński G., Gieren W., Soszyński I., Bresolin F., Kudritzki R.-P., Dall'Ora M., Storm J., Bono G., 2006, ApJ, 642, 216
Poole T. S. et al., 2008, MNRAS, 383, 627
Prialnik D., 1986, ApJ, 310, 222
Roming P. W. A. et al., 2005, Space Sci. Rev., 120, 95
Sandage A., 1971, ApJ, 166, 13
Schlafly E. F., Finkbeiner D. P., 2011, ApJ, 737, 103
Scowcroft V., Freedman W. L., Madore B. F., Monson A. J., Persson S. E., Seibert M., Rigby J. R., Melbourne J., 2013, ApJ, 773, 106
Sekiguchi K., Kilkenny D., Winkler H., Doyle J. G., 1989, MNRAS, 241, 827
Shafter A. W., 2013, AJ, 145, 117
Shafter A. W., Rau A., Quimby R. M., Kasliwal M. M., Bode M. F., Darnley M. J., Misselt K. A., 2009, ApJ, 690, 1148
Shafter A. W. et al., 2011, ApJ, 734, 12
Shafter A. W., Darnley M. J., Bode M. F., Ciardullo R., 2012, ApJ, 752, 156
Shara M. M. et al., 2016, ApJS, 227, 1
Shara M. M. et al., 2017, MNRAS, preprint (arXiv:1702.06988)
Shields G. A., 1974, ApJ, 191, 309
Shore S. N. et al., 2013, Astron. Telegram, 5378
Skillman E. D. et al., 2014, ApJ, 786, 44
Skrutskie M. F. et al., 2006, AJ, 131, 1163
Smith H. J., 1954, AJ, 59, 193
Starrfield S., Truran J. W., Sparks W. M., Kutter G. S., 1972, ApJ, 176, 169
Starrfield S., Truran J. W., Sparks W. M., Arnould M., 1978, ApJ, 222, 600
Steele I. A. et al., 2004, in Oschmann J. M., Jr, ed., Proc. SPIE Conf. Ser. Vol. 5489, Ground-based Telescopes. SPIE, Bellingham, p. 679
Surina F., Hounsell R. A., Bode M. F., Darnley M. J., Harman D. J., Walter F. M., 2014, AJ, 147, 107
Tajitsu A., Sadakane K., Naito H., Arai A., Aoki W., 2015, Nature, 518, 381
Tajitsu A., Sadakane K., Naito H., Arai A., Kawakita H., Aoki W., 2016, ApJ, 818, 191
Tody D., 1986, in Crawford D. L., ed., Proc. SPIE Conf. Ser. Vol. 627, Instrumentation in astronomy VI. SPIE, Bellingham, p. 733
Udalski A., Wyrzykowski L., Pietrzynski G., Szewczyk O., Szymanski M., Kubiak M., Soszynski I., Zebrun K., 2001, AcA, 51, 221
van den Bergh S., 2000, The Galaxies of the Local Group. Cambridge Univ. Press, Cambridge
Walker M. F., 1954, PASP, 66, 230
Whelan J., Iben Jr I., 1973, ApJ, 186, 1007
Williams R. E., 1992, AJ, 104, 725
Williams R., 2012, AJ, 144, 98

Williams S. C., Darnley M. J., 2015, Astron. Telegram, 8061
Williams S. C., Darnley M. J., 2016, Astron. Telegram, 9628
Williams R. E., Hamuy M., Phillips M. M., Heathcote S. R., Wells L., Navarrete M., 1991, ApJ, 376, 721
Williams S. C., Darnley M. J., Bode M. F., Keen A., Shafter A. W., 2014, ApJS, 213, 10
Williams S. C., Darnley M. J., Bode M. F., Shafter A. W., 2016, ApJ, 817, 143
Woudt P. A., Ribeiro V. A. R. M. eds, 2014, ASP Conf. Ser. Vol. 490: Stella Novae: Past and Future Decades. Astron. Soc. Pac., San Francisco
Wright W. H., 1940, Publications of Lick Observatory, 14, 27
Wright A. E., Barlow M. J., 1975, MNRAS, 170, 41

APPENDIX A: NUV, OPTICAL AND NIR PHOTOMETRY OF NOVA IC 1613 2015

Table A1. Near-UV, optical and near-IR photometry of Nova IC 1613 2015. These data have not been corrected for any reddening.

Date (UT)	t (d)	Telescope and instrument	Exposure (s)	Filter	Photometry
2016 September 20.993	10.513	LT IO:O	180	u'	18.078 ± 0.033
2016 September 21.978	11.498	LT IO:O	120	u'	17.954 ± 0.038
2016 September 25.046	14.566	LT IO:O	180	u'	18.618 ± 0.048
2016 September 25.948	15.468	LT IO:O	180	u'	18.653 ± 0.064
2016 September 27.036	16.556	LT IO:O	360	u'	18.583 ± 0.053
2016 September 30.962	20.482	LT IO:O	360	u'	18.894 ± 0.044
2016 October 06.009	25.529	LT IO:O	240	u'	19.181 ± 0.030
2016 October 08.078	27.598	LT IO:O	360	u'	19.353 ± 0.029
2016 October 09.014	28.534	LT IO:O	360	u'	19.396 ± 0.028
2016 October 13.014	32.534	LT IO:O	360	u'	19.527 ± 0.031
2016 November 03.995	54.515	LT IO:O	360	u'	20.317 ± 0.036
2016 November 07.983	58.503	LT IO:O	360	u'	20.421 ± 0.040
2016 November 15.967	66.487	LT IO:O	360	u'	20.741 ± 0.040
2016 December 12.868	93.388	LT IO:O	360	u'	21.554 ± 0.062
2016 September 12.087	1.607	LT IO:O	180	B	16.827 ± 0.038
2016 September 14.043	3.563	LT IO:O	60	B	17.171 ± 0.038
2016 September 17.114	6.634	LT IO:O	60	B	17.675 ± 0.038
2016 September 20.996	10.516	LT IO:O	180	B	18.252 ± 0.038
2016 September 21.981	11.501	LT IO:O	120	B	18.226 ± 0.039
2016 September 24.606	14.126	LCO 2 m Spectral	360	B	18.927 ± 0.068
2016 September 25.049	14.569	LT IO:O	180	B	18.764 ± 0.051
2016 September 25.951	15.471	LT IO:O	180	B	18.925 ± 0.047
2016 September 27.057	16.577	LT IO:O	180	B	18.816 ± 0.050
2016 September 29.929	19.449	LT IO:O	180	B	18.932 ± 0.055
2016 October 3.576	23.096	LCO 2 m Spectral	360	B	19.461 ± 0.045
2016 October 05.994	25.514	LT IO:O	180	B	19.430 ± 0.039
2016 October 08.062	27.582	LT IO:O	180	B	19.567 ± 0.039
2016 October 08.999	28.519	LT IO:O	180	B	19.579 ± 0.039
2016 October 10.920	30.440	LT IO:O	180	B	19.671 ± 0.042
2016 October 12.999	32.519	LT IO:O	180	B	19.803 ± 0.040
2016 October 18.969	38.489	LT IO:O	180	B	20.041 ± 0.065
2016 October 20.530	40.050	LCO 2 m Spectral	360	B	20.154 ± 0.073
2016 October 30.038	49.558	LT IO:O	180	B	20.275 ± 0.063
2016 November 03.980	54.500	LT IO:O	180	B	20.362 ± 0.043
2016 November 07.969	58.489	LT IO:O	180	B	20.500 ± 0.046
2016 November 15.951	66.471	LT IO:O	120	B	20.698 ± 0.052
2016 December 12.845	93.365	LT IO:O	240	B	21.255 ± 0.048
2016 September 12.090	1.610	LT IO:O	180	V	16.651 ± 0.041
2016 September 14.044	3.564	LT IO:O	60	V	16.885 ± 0.041
2016 September 17.115	6.635	LT IO:O	60	V	17.493 ± 0.041
2016 September 18.499	8.020	LCO 2 m Spectral	360	V	17.953 ± 0.058
2016 September 20.978	10.498	LT IO:O	180	V	18.122 ± 0.041
2016 September 21.984	11.504	LT IO:O	180	V	18.118 ± 0.037
2016 September 24.611	14.131	LCO 2 m Spectral	360	V	18.722 ± 0.056
2016 September 25.051	14.571	LT IO:O	180	V	18.716 ± 0.045
2016 September 25.954	15.474	LT IO:O	120	V	18.767 ± 0.051
2016 September 27.061	16.581	LT IO:O	180	V	18.749 ± 0.047
2016 September 29.934	19.454	LT IO:O	180	V	19.012 ± 0.051
2016 September 30.949	20.469	LT IO:O	180	V	19.078 ± 0.045
2016 October 03.580	23.100	LCO 2 m Spectral	360	V	19.418 ± 0.048
2016 October 05.996	25.516	LT IO:O	180	V	19.457 ± 0.042
2016 October 09.001	28.521	LT IO:O	180	V	19.729 ± 0.043

Table A1 – *continued*

Date (UT)	t (d)	Telescope and instrument	Exposure (s)	Filter	Photometry
2016 October 10.923	30.443	LT IO:O	180	V	19.791 ± 0.044
2016 October 13.002	32.522	LT IO:O	180	V	19.939 ± 0.044
2016 October 18.974	38.494	LT IO:O	120	V	20.077 ± 0.050
2016 October 20.536	40.056	LCO 2 m Spectral	360	V	20.147 ± 0.077
2016 October 30.041	49.561	LT IO:O	180	V	20.343 ± 0.101
2016 November 03.983	54.503	LT IO:O	180	V	20.588 ± 0.060
2016 November 07.972	58.492	LT IO:O	180	V	20.485 ± 0.079
2016 November 15.954	66.474	LT IO:O	180	V	20.696 ± 0.069
2016 December 12.849	93.369	LT IO:O	300	V	21.089 ± 0.052
2016 September 18.503	8.023	LCO 2 m Spectral	180	r'	17.309 ± 0.015
2016 September 21.002	10.522	LT IO:O	180	r'	17.550 ± 0.005
2016 September 21.987	11.507	LT IO:O	120	r'	17.537 ± 0.006
2016 September 24.616	14.136	LCO 2 m Spectral	360	r'	17.967 ± 0.013
2016 September 25.054	14.574	LT IO:O	180	r'	17.962 ± 0.009
2016 September 25.957	15.477	LT IO:O	180	r'	18.032 ± 0.011
2016 September 27.062	16.582	LT IO:O	180	r'	18.051 ± 0.012
2016 September 29.938	19.458	LT IO:O	180	r'	18.277 ± 0.030
2016 September 30.952	20.472	LT IO:O	180	r'	18.314 ± 0.010
2016 October 03.585	23.105	LCO 2 m Spectral	360	r'	18.371 ± 0.009
2016 October 05.999	25.519	LT IO:O	60	r'	18.453 ± 0.009
2016 October 08.068	27.588	LT IO:O	180	r'	18.532 ± 0.007
2016 October 09.004	28.524	LT IO:O	180	r'	18.554 ± 0.006
2016 October 10.925	30.445	LT IO:O	120	r'	18.579 ± 0.009
2016 October 13.004	32.524	LT IO:O	180	r'	18.651 ± 0.007
2016 October 18.976	38.496	LT IO:O	180	r'	18.845 ± 0.012
2016 October 20.541	40.061	LCO 2 m Spectral	360	r'	18.892 ± 0.015
2016 October 30.044	49.564	LT IO:O	180	r'	19.269 ± 0.017
2016 November 03.985	54.505	LT IO:O	60	r'	19.487 ± 0.021
2016 November 07.974	58.494	LT IO:O	180	r'	19.614 ± 0.016
2016 November 15.957	66.477	LT IO:O	180	r'	20.003 ± 0.016
2016 December 12.853	93.373	LT IO:O	240	r'	20.881 ± 0.026
2016 September 12.094	1.614	LT IO:O	360	i'	16.891 ± 0.007
2016 September 14.045	3.565	LT IO:O	60	i'	16.762 ± 0.008
2016 September 17.116	6.636	LT IO:O	60	i'	17.185 ± 0.008
2016 September 18.506	8.026	LCO 2 m Spectral	180	i'	17.462 ± 0.018
2016 September 21.005	10.525	LT IO:O	180	i'	17.830 ± 0.007
2016 September 21.990	11.510	LT IO:O	180	i'	17.877 ± 0.007
2016 September 24.621	14.141	LCO 2 m Spectral	360	i'	18.427 ± 0.021
2016 September 25.057	14.577	LT IO:O	180	i'	18.425 ± 0.011
2016 September 25.960	15.480	LT IO:O	180	i'	18.509 ± 0.015
2016 September 27.065	16.585	LT IO:O	180	i'	18.553 ± 0.019
2016 September 29.941	19.461	LT IO:O	180	i'	18.814 ± 0.021
2016 September 30.955	20.475	LT IO:O	180	i'	18.899 ± 0.017
2016 October 03.590	23.110	LCO 2 m Spectral	360	i'	19.144 ± 0.019
2016 October 06.002	25.522	LT IO:O	180	i'	19.243 ± 0.012
2016 October 08.071	27.591	LT IO:O	180	i'	19.400 ± 0.013
2016 October 09.007	28.527	LT IO:O	180	i'	19.444 ± 0.013
2016 October 10.928	30.448	LT IO:O	180	i'	19.529 ± 0.019
2016 October 13.007	32.527	LT IO:O	180	i'	19.642 ± 0.016
2016 October 20.544	40.064	LCO 2 m Spectral	360	i'	20.013 ± 0.051
2016 October 30.047	49.567	LT IO:O	180	i'	20.415 ± 0.047
2016 November 03.988	54.508	LT IO:O	180	i'	20.548 ± 0.038
2016 November 07.977	58.497	LT IO:O	180	i'	20.596 ± 0.049
2016 November 15.960	66.480	LT IO:O	180	i'	20.832 ± 0.049
2016 December 12.866	93.386	LT IO:O	300	i'	21.248 ± 0.138
2016 September 21.008	10.528	LT IO:O	180	z'	17.431 ± 0.015
2016 September 21.993	11.513	LT IO:O	120	z'	17.443 ± 0.015
2016 September 25.060	14.580	LT IO:O	180	z'	17.820 ± 0.018
2016 September 25.963	15.483	LT IO:O	180	z'	17.879 ± 0.027
2016 September 27.068	16.588	LT IO:O	180	z'	17.904 ± 0.022
2016 September 27.940	17.460	LT IO:O	180	z'	17.990 ± 0.039
2016 September 29.944	19.464	LT IO:O	180	z'	18.065 ± 0.023
2016 September 30.958	20.478	LT IO:O	180	z'	18.078 ± 0.019

Table A1 – *continued*

Date (UT)	t (d)	Telescope and instrument	Exposure (s)	Filter	Photometry
2016 October 06.005	25.525	LT IO:O	120	z'	18.172 ± 0.018
2016 October 08.074	27.594	LT IO:O	120	z'	18.322 ± 0.019
2016 October 09.010	28.530	LT IO:O	180	z'	18.337 ± 0.016
2016 October 13.010	32.530	LT IO:O	180	z'	18.556 ± 0.018
2016 October 18.981	38.501	LT IO:O	180	z'	18.950 ± 0.050
2016 October 30.050	49.570	LT IO:O	120	z'	19.689 ± 0.089
2016 November 03.992	54.512	LT IO:O	180	z'	19.940 ± 0.085
2016 November 07.980	58.500	LT IO:O	180	z'	20.057 ± 0.106
2016 November 15.963	66.483	LT IO:O	180	z'	20.536 ± 0.084
2016 December 12.863	93.383	LT IO:O	300	z'	21.366 ± 0.120
2016 September 19.191	8.711	LT IO:I	538	H	16.598 ± 0.103
2016 September 21.043	10.563	LT IO:I	538	H	16.991 ± 0.117
2016 September 25.066	14.586	LT IO:I	538	H	17.678 ± 0.102
2016 October 08.965	28.485	LT IO:I	538	H	18.772 ± 0.143

This paper has been typeset from a TEX/LATEX file prepared by the author.